

DISCLAIMER

This report was prepared as an account of work sponsored by an agency of the United States Government. Neither the United States Government nor any agency thereof, nor any of their employees, makes any warranty, expressed or implied, or assumes any legal liability or responsibility for the accuracy, completeness, or usefulness of any information, apparatus, product, or process disclosed, or represents that its use would not infringe privately owned rights. Reference herein to any specific commercial product, process, or service by trade name, trademark, manufacturer, or otherwise does not necessarily constitute or imply its endorsement, recommendation, or favoring by the United States Government or any agency thereof. The views and opinions of authors expressed herein do not necessarily state or reflect those of the United States Government.

This report has been reproduced directly from the best available copy.

Available to DOE and DOE contractors from the Office of Scientific and Technical Information, P.O. Box 62, Oak Ridge, TN 37831; prices available from (615) 576-8401.

Available to the public from the National Technical Information Service, U.S. Department of Commerce, 5285 Port Royal Rd., Springfield VA 22161

DOE/BC/95000153
Distribution Category UC-122

Electrical and Electromagnetic Methods for
Reservoir Description and Process Monitoring

By
H. Frank Morrison
Ki Ha Lee
Alex Becker

July 1995

Prepared for
U.S. Department of Energy
Assistant Secretary for Fossil Energy

R. E. Lemmon, Project Manager
Bartlesville Project Office
P.O. Box 1398
Bartlesville, OK 74005

Prepared by
University of California
Lawrence Berkeley Laboratory
Berkeley, CA 94720

INTRODUCTION

One of important geophysical parameters that can be used to help monitor and characterize a petroleum reservoir is the electrical conductivity. The electrical conductivity of rock is dominantly a function of fluid type, its saturation, the porosity, and hydraulic permeability of the rock. For these reasons, resistivity well logs have long been used by geologists and reservoir engineers in petroleum industries to map variations in pore fluid, to distinguish between rock types, and to determine completion intervals in wells. It is therefore a natural extension to use the electrical conductivity structure to provide additional information about the reservoir. Reservoir simulation and process monitoring rely heavily on the physical characteristics of the reservoir model. At present, numerical codes use point measurements of porosity, permeability, and fluid saturation and extrapolate these data throughout a three-dimensional (3-D) grid. The knowledge of a high-resolution geophysical parameter such as electrical conductivity would aid this extrapolation and improve the reservoir simulation effort. In addition, since conductivity is sensitive to changes in the composition and state of fluids in pores and fractures it becomes an ideal method for monitoring a reservoir process.

During FY-91 a coordinated electrical and electromagnetic (em) geophysical research program for petroleum reservoir characterization and process monitoring was initiated. Parties involved in this program include Lawrence Berkeley Laboratory (LBL), Lawrence Livermore Laboratory (LLNL), Sandia National Laboratory (SNL), and University of California at Berkeley (UCB). The overall objectives of the program are:

- To integrate research funded by DOE for hydrocarbon recovery into a focused effort to demonstrate the technology in the shortest time with the least cost.
- To assure industry acceptance of the technology developed by having industry involvement in the planning, implementation, and funding of the research.
- To focus the research on real world problems that have the potential for solution in the near term with significant energy payoff.

Specific research activities conducted through this integrated effort have been in the following five general areas:

- 1) em modeling development.
- 2) Data interpretation methods development.
- 3) Hardware and instrumentation development.
- 4) EOR and reservoir characterization.
- 5) Controlled field experiments.

At LBL/UCB research has been focused on activities 1), 2), and 5) in FY92. The primary focus of these activities is in the development of reliable inversion and imaging schemes that can yield conductivity distributions from measured electrical and em field data. The development of accurate forward modeling algorithms and the high-quality scale model experiment are necessarily the early part of the field experiment design and the inversion scheme development for ultimately monitoring the front tracking in existing reservoirs.

SUMMARY OF TECHNICAL PROGRESS

• Time-domain electromagnetic (TEM) scale model

As an integral part of the joint R&D program for petroleum reservoir characterization and process monitoring, we are continuing development of a TEM scale model of the Richmond Field Station (RFS). The scale model study is important because it can be used to simulate reservoir models in a controlled environment. A more immediate objective of developing the scale model is to obtain high-quality (low noise, high bandwidth, high dynamic range) data for the q-domain imaging algorithm (Lee and Xie, 1993) currently under development at LBL. Finally the scale model parameters will be very useful in the design of full scale field instrumentation.

The scale model consists of a 1.2 m diameter, 0.5 m thick, cylindrical graphite block with an electrical conductivity of about 80,000 S/m. The experiments are done on such a scale that 1 cm in the scale model is equivalent to 8 m in real world. The model represents a field environment with an average background resistivity of 8 ohm-m so that the transmitted and received wave forms are observed on an identical time scale to that which would be used in a full scale field experiment.

The 1992 effort was mainly directed at improving the scale model equipment. A very important step in this direction was the execution of a computer program that can be used to evaluate the effects of the model EM system parameters such as bandwidth and dynamic range on the observed scale model response. The program was written in Math CAD 3.0 and allows the introduction of all technical details such as transmitter moment, inductance and resistance and the receiver capture area as well as its damping and distributed capacitance. Even the effects of cabling parameters can be included. The test geophysical signal for the simulation program is the ideal (theoretical) whole space response.

Based on system simulations and other experimental work we made many equipment changes to the 1991 (Figure 1) configuration of the scale model instrumentation. These include replacement of the transmitter and receiver coils to increase the sensitivity and signal to noise ratio. We also replaced the primary field signal generator (HP 3325) by a robust Geonics EM-47 unit which enabled us to increase the transmitter moment by about an order of magnitude and the removal of the noisy preamplifier. Finally we significantly improved the data acquisition process by switching to a 486 based PC from the older 386 model and by amending the data acquisition control program. The Analogic 6400 (1 MHz 14 bit) A/D converter was retained.

• Inversion and imaging of em data

One of the principal goals of electromagnetic reservoir geophysics is to obtain high resolution images of subsurface electrical properties. From these images of conductivity and/or permittivity, information about reservoir heterogeneity and fluid distribution can be deduced and used to estimate oil field properties such as porosity, fracture orientation,

amount of oil present in situ, and improve the design and monitoring of enhanced oil recovery processes. In this report we describe the status of the following two independent imaging algorithm development.

a) Iterative Born inversion

Since the initial development reported in the FY91 Annual Report (December 1991), the iterative Born inversion algorithm has been under continuous development, and its initial test has been made using data collected from the University of California's Richmond Field Station (RFS). The detailed description of the application of the method is given in the 'controlled field experiment' section.

b) Development in the wave-field analysis

It has been shown in the FY91 Annual Report (December 1991) that diffusion-to-wavefield transform can be achieved using approximately 1.5 decades of time-domain data, and that reasonably accurate traveltimes can be obtained from the wavefields thus constructed. The velocity of the wavefield in the q domain is inversely proportional to the square root of the conductivity. So the slowness is proportional to the square root of the conductivity. We invert traveltimes for the slowness distribution using a nonlinear iterative tomographic algorithm. Each iteration consists of two main parts. The first part finds raypaths for a given slowness model. The second part updates the slowness model using the raypaths computed in the first part. The updating algorithm uses a regularization scheme based on mixed constraints. The tomographic algorithm is based on Fermat's principle and the detailed description of the development is shown in the paper by Lee and Xie (1993).

To test the traveltimes tomography algorithm for its convergence a numerical simulation has been carried out using the simple model shown in Figure 2. A total of 21 sources and 21 receivers were used for the simulation with a constant spacing of 10 m. For a low-contrast conductivity distribution with $\sigma_1=0.02$ S/m and $\sigma_2=\sigma_3=0.05$ S/m, frequency-domain magnetic fields were first computed at each receiver site and inverse Fourier transformed to the time domain. The window of time-domain data used for the transform was $10 \mu\text{s} \sim 0.5$ ms throughout.

The transient fields and transformed wavefields for three (among 21) source points, with source locations at $z=0, 100,$ and 200 m, are shown in Figure 3. Figures 4 and 5 show computed raypaths from five (among 21) selected source points (at $z=0, 50, 100, 150,$ and 200 m) to all 21 receiver points and the corresponding conductivity tomogram at the end of 20th iteration, respectively. There is an indication of a triangular-shaped conductive region on the upper-right corner of the tomogram, but the overall image is blurred. At the end of 40th iteration, the general trend of computed raypaths (Figure 6) seems more reasonable, and the conductivity image (Figure 7) becomes closer to the original model. By the 68th iteration, we have been able to obtain perfectly reasonable raypaths (Figure 8) along with a clear conductivity tomogram (Figure 9). The computed raypaths are straight in homogeneous regions and they seem to bend smoothly near the inhomogeneous boundary.

Total computational effort involved in this tomographic inversion was approximately 3 CPU hours on a SUN SPARCstation 2.

With the convergence test successfully concluded on a simple model of small contrast, we are now engaged in upgrading the numerical code for testing more realistic, higher contrast models of complicated conductivity distribution.

• **Controlled field experiments**

Since 1988, a series of salt water injection experiments have been conducted at RFS to evaluate the use of different geophysical methods for monitoring the injection process and for determining the geometry of the resulting plume. The latest 1992 experiment employed the cross borehole configuration. After an initial system setup and debugging session, a baseline crosshole em data set was collected in May, 1992. It consisted of four crosshole profiles with the transmitter in the central well (INJ1) and the receiver tool deployed in each of the four em observation holes (See Figure 10). Data were collected at a frequency of 18,500 Hz using a transmitter tool spacing of 0.5 m from the surface to a depth of 60 m for each receiver position. Receiver stations were spaced 5 m apart from 5 m to 55 m in each of the four observation holes. Next, a volume of water was pumped into a 100,000 gallon holding pond and mixed with salt until the water conductivity was raised to 1 S/m. The fluid was then injected into borehole INJ1 at a rate of 10 gallons per minute for about 4 days. Assuming a porosity of 30 percent, the injected water would sweep a cylindrical space 3 m high and 8 m in radius. We collected a second set of crosshole em and induction logging data during a four week period in June following the injection.

After the June measurements were made, fluid was pumped out of well INJ1 until the water conductivity was restored to the background value it had before the experiment began (60 mS/m). The total volume pumped out was 300,000 gallons, about 6 times the amount injected. The pumping began on July 6 at a rate of 20 gallons per minute and it lasted 12 days. Water levels in the wells open to the aquifer were monitored during this period to better understand the hydrology of the site. The water was pumped into a drain that flows into San Francisco Bay. Finally after a two-week period which allowed the water level to recover its original position we attempted to repeat the baseline em measurements in the EMNE well. Unfortunately, due to instrument problems data quality was much poorer than in May and this data was not retained. In all, the experiment was conducted over a period of three months.

The overall system deployment was very similar to that described by Wilt et al. (1991), with the exception that an audio power amplifier (Crown model 610) was used for signal power amplification instead of the Zonge GGT-20 transmitter. The Crown amplifier has a high frequency limit in excess of 20,000 Hz, whereas the Zonge transmitter was limited to 8,000 Hz. This higher frequency capability is essential at RFS because the boreholes are closely spaced and the background resistivity is relatively high (~20 ohm-m). Other changes included the use of lightweight, portable winches, short segments of logging cable and the use of a special transmitter cable capable of carrying 10 amps of current.

In general, we found that the data repeatability and reciprocity errors for the RFS 1992 experiment were two to three times worse than those at Devine, Texas (Wilt et al. 1991). We feel that the noise level is higher at Richmond because of the higher frequencies involved and closer physical proximity of the source and receiver instrument vans. Both of these factors allow for variable surficial coupling of the high level transmitter signal to the receiver. Although considerable time was spent before both the Devine and Richmond tests removing 'ground-loops' from our system, additional errors (and ground loops) were evident in the Richmond data, primarily as the result of these more difficult operating conditions. Secondly, because Richmond is located in an industrial area, external noise (from grounded power lines, BART etc.) is more of a problem and constitutes an unknown source of error.

a) Crosshole em profiles

Ten sets of cross-well data were collected with the transmitter in INJ1 and the receiver in each of the four surrounding em wells. Four of these data sets were collected before injection and six after injection. In order to present all the data in any one cross-well set simultaneously, they were first normalized to a source strength of unit dipole moment. Then the amplitude and phase were plotted in a gray scale format as a function of transmitter and receiver position. Figures 11 and 12 show the EMNW data sets before and after injection, respectively. Plotting the data in this manner allows us to check for data continuity between profiles and also determine any change that takes place due to the injection.

Figures 11 and 12 clearly show the data both before and after injection to be smoothly varying both along each individual profile and in between the individual lines. Although the magnitudes of the changes are not spectacular, a decrease in amplitude and an increase in phase can be seen at a transmitter depth of approximately 30 m when the post-injection data is compared to the pre-injection data. These changes are caused by the injection of salt water and are consistent with models run in the design phase of the experiment.

The effects of the injection become much more apparent if we calculate the secondary fields resulting from the introduction of the plume. This is a simple process involving the subtraction of the fields measured before the injection from those measured after injection. The resulting anomalies shown in Figure 13 clearly indicate large changes that are not readily apparent in the raw data. The fact that the anomalies are several times larger than the noise estimates suggests that the EMNW data are of sufficient quality to be used in various imaging schemes.

It was noticed both during the data collection as well as during the processing that the data quality appeared to decrease in a clockwise fashion from the EMNW well to the EMSW well. This can be displayed by calculating the secondary fields in the EMSW data resulting from the salt water injection. Although the pre-injection and post-injection data appear to be fairly consistent, the secondary fields (Figure 14) do not show the same character as those in the EMNW data. This may be due in part to noisier data, but also could result from the plume moving away from INJ1 in a northerly direction as suggested by earlier

experiments (Bevc and Morrison, 1991) rather than spreading symmetrically about the injection well. Comparing these results with those obtained in the EMNE and EMSE wells suggests that this may be the case as the EMNE data show a large anomaly resembling the one present in the EMNW data while the EMSE data show results similar to the EMSW measurements.

b) Interpretation of data

One of the prime considerations of the Richmond experiment was to produce a data set in which the geology, to a first order, exhibits a geometry suitable for our 2-D inversion routine (Alumbaugh and Morrison, 1992). This routine assumes a cylindrical symmetry of the conductivity distribution about the transmitter borehole in an otherwise homogenous half space. It uses an iterative Born scheme to linearize the problem and regularized least squares to invert for the conductivity distribution.

Because the Richmond geology consists of interbedded conductive shales and sands overlying a more resistive basement, the plume can't be interpreted as being injected into a homogenous half space. Thus rather than inverting only for changes in conductivity resulting from the injection, the entire conductivity structure between the two wells was imaged both before and after injection and the results compared. The background conductivity used in the process was chosen by finding the homogeneous half space that minimizes the magnitude of the secondary field.

Figure 15 shows the images obtained by inverting the pre- and post-injection data collected in the EMNW well. Though it does not indicate flat lying layers, the pre-injection image does show conductive overburden overlying a more resistive basement. The post-injection image clearly shows a high conductivity anomaly that corresponds to the injection zone. This strongly suggests that the salt water has migrated to the northwest which agrees very well with the results published by Bevc and Morrison (1991). Inversions of the other data support this conclusion. Images of the EMNE data indicate some migration to the northeast while the EMSW inversions indicate almost no migration to the southwest. The direction of plume migration becomes even more apparent if we plot the change in conductivity between the before and after images as shown in Figure 16.

Notice that the inversions from EMSE have not been included here. This is due to the fact that the average misfits to these data was over 20 % compared to 10 % or less for data collected in the other three wells. This large misfit may be due to extreme 3-D geology between the two wells, poor data quality, or a combination of both.

c) Conclusions

The 1992 Richmond field experiment showed that a salt water injection process can be monitored using cross-well electromagnetics. Although the cross-well em system worked fairly well there is definite room for improvement as there were significant drift problems and repeatability errors. However, even with these problems the data is in most cases of sufficient quality not only to detect the presence of the body but also to allow for simple

imaging schemes to be applied. Results from this imaging process correlate well with previous experiments which show the plume to be moving off to the northwest. Additional 3-D modeling needs to be done both to verify this as well as to test the limits of the 2-D inversion code.

REFERENCES

Alumbaugh D.L., and H.F. Morrison, 1992, Tomographic Imaging of Cross well EM Data: Extended abstracts from the Society of Exploration Geophysicists 1992 annual meeting, New Orleans, Louisiana.

Bevc, D. and H.F. Morrison, 1991, Borehole-to-surface electrical conductivity monitoring of a salt water Injection experiment: *Geophysics* 56 no. 6 p 769-777.

Electrical and Electromagnetic Methods for Reservoir Description and Process Monitoring, December 1991, Annual Report to Bartlesville Project Office, Lawrence Berkeley Laboratory.

Lee, K. H., and G. Q. Xie, 1993, A new approach to imaging with low-frequency electromagnetic fields: Accepted for publication in the June issue of *Geophysics*.

Wilt, M.J., H.F. Morrison, A. Becker, and K.H. Lee, 1991, Cross-borehole and surface-to-borehole electromagnetic induction for reservoir characterization: DOE report DOE/BC/91002253.

Wilt, M.J., D.L. Alumbaugh, H.F. Morrison, A. Becker, K.H. Lee, and M. Deszcz-Pan, Crosshole Electromagnetic Imaging for Reservoir Definition and Monitoring, July 1993, LBL-34734.

Crosshole TEM Scale Model

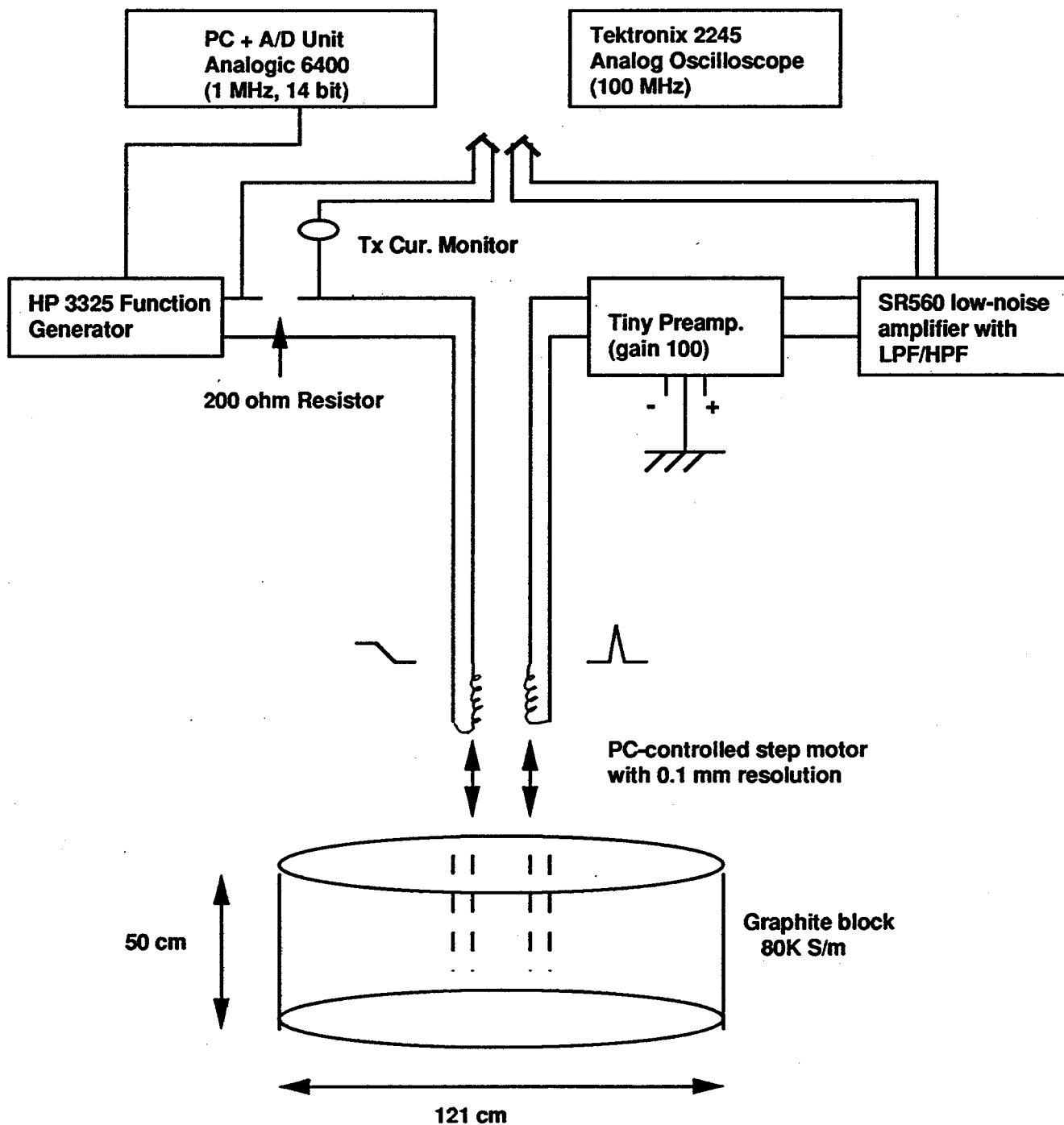


Figure 1. Block diagram for the crosshole TEM scale model (1991 configuration)

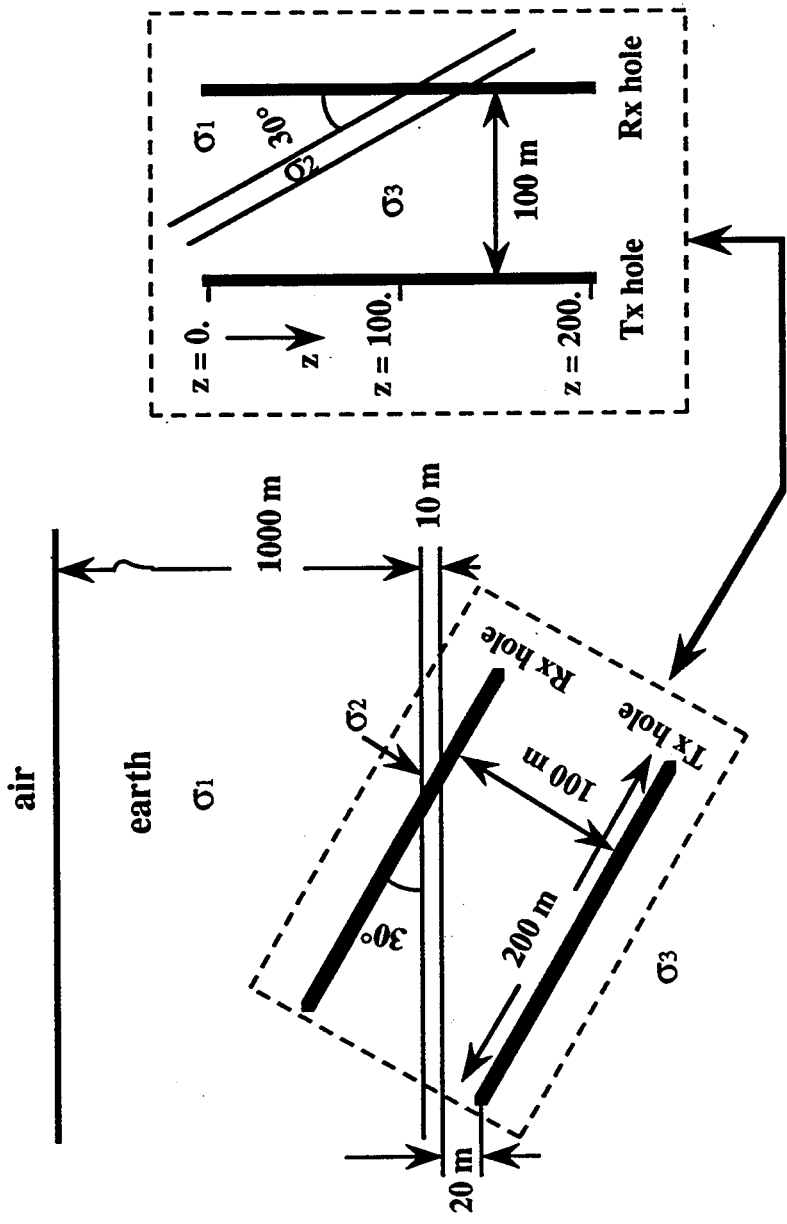


Figure 2. Simple 1-D model for testing tomographic algorithm

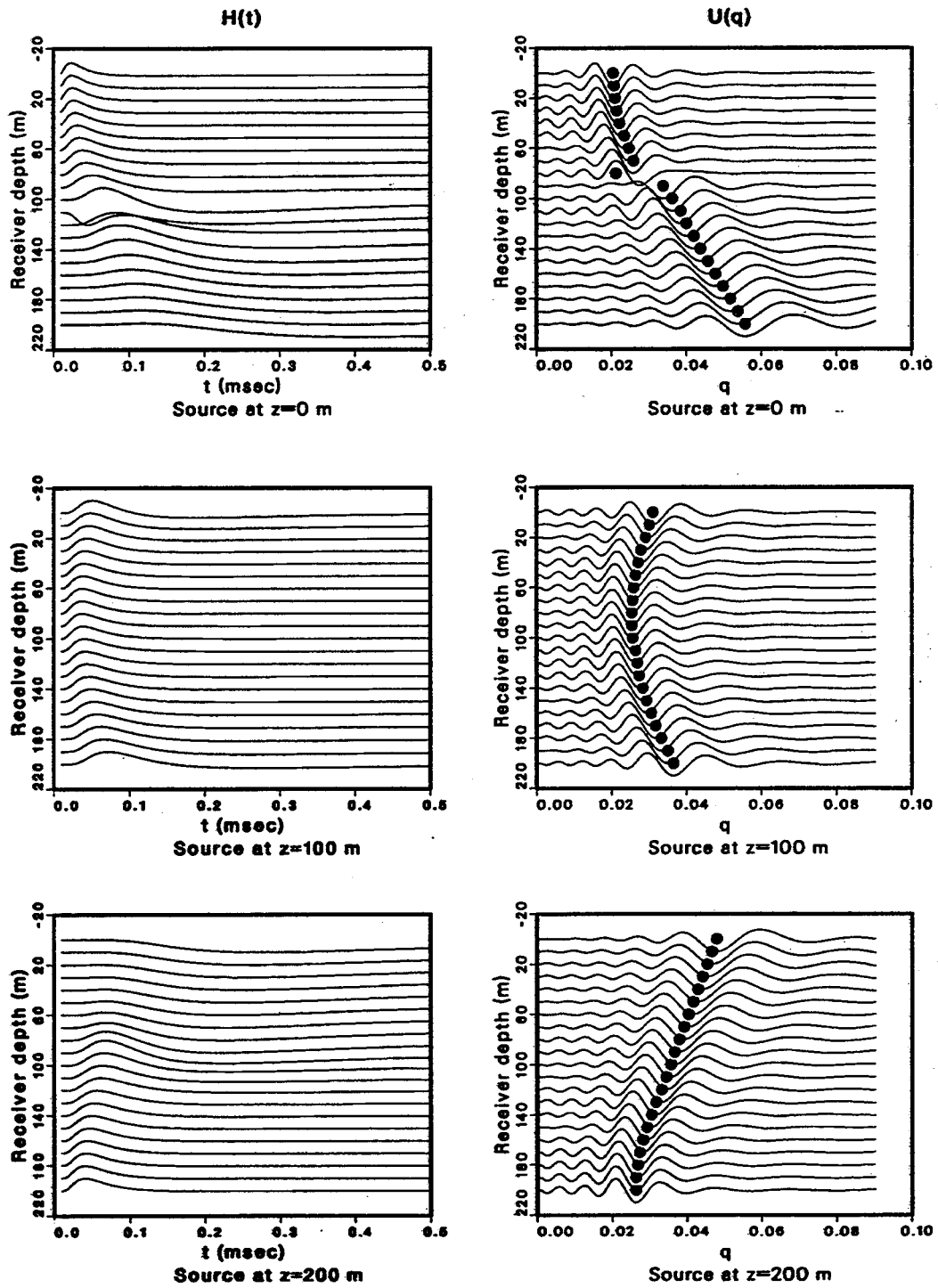


Figure 3. Transient magnetic fields at 21 receiver positions due to sources at $z=0$, 100, and 200 m, respectively, and their corresponding wavefields.

Wave-Field Ray Paths

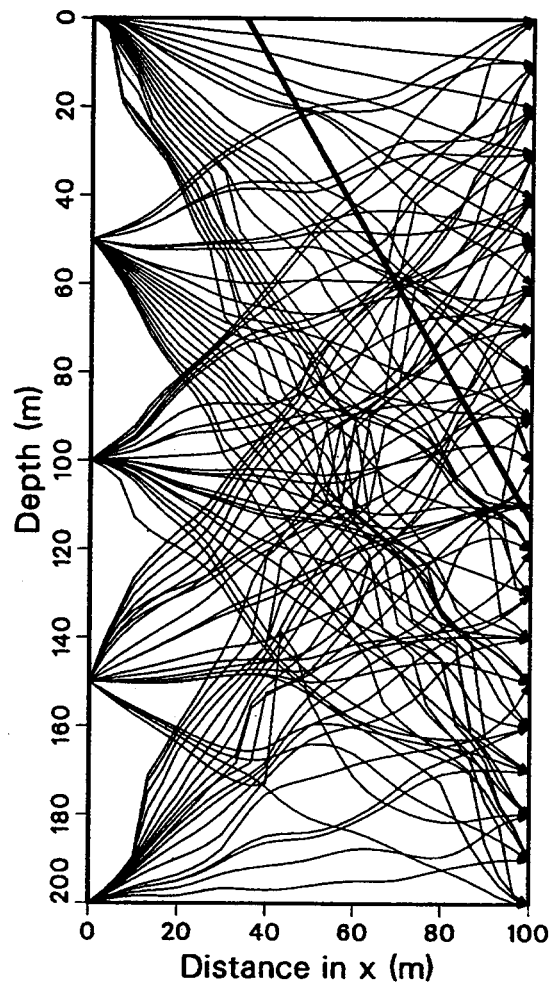


Figure 4. Raypaths from five sources at $z=0$, 50, 100, 150, and 200 m to 21 receivers, after 20 iterations.

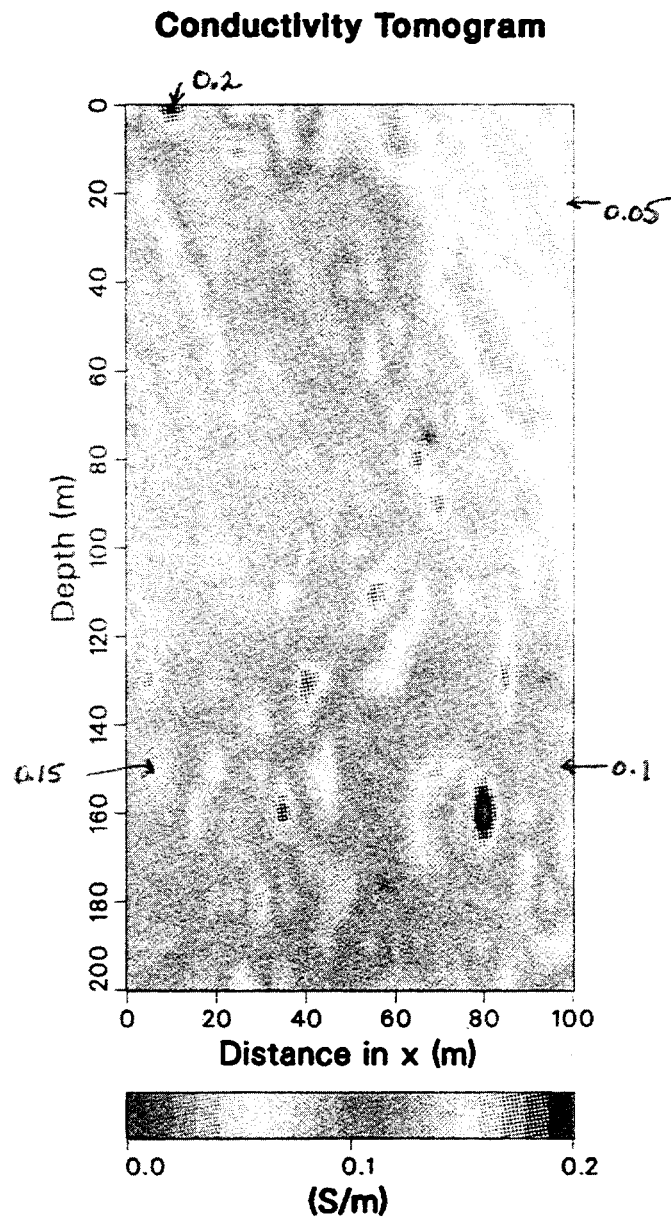


Figure 5. Conductivity tomogram after 20 iterations.

Wave-Field Ray Paths

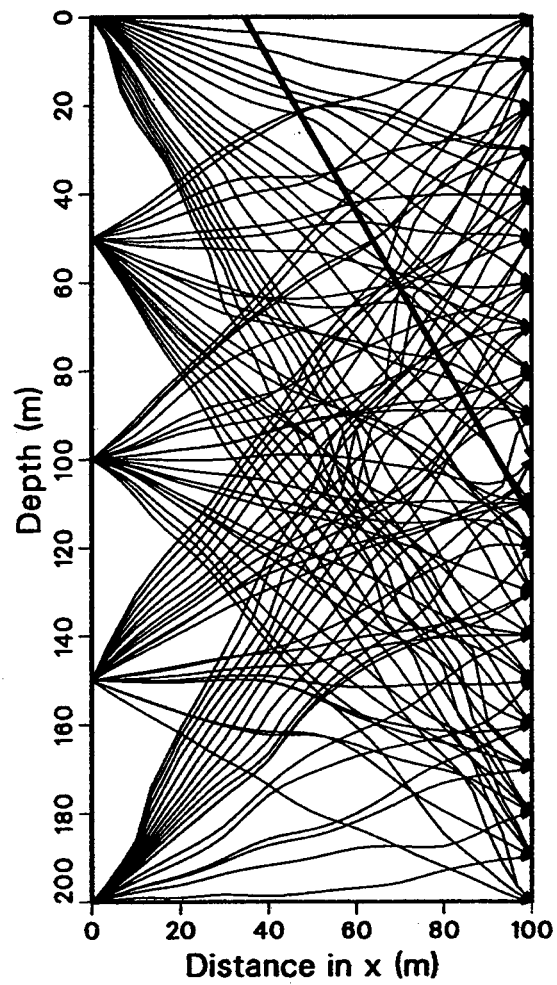


Figure 6. Raypaths from five sources at $z=0$, 50, 100, 150, and 200 m to 21 receivers, after 40 iterations.

Conductivity Tomogram

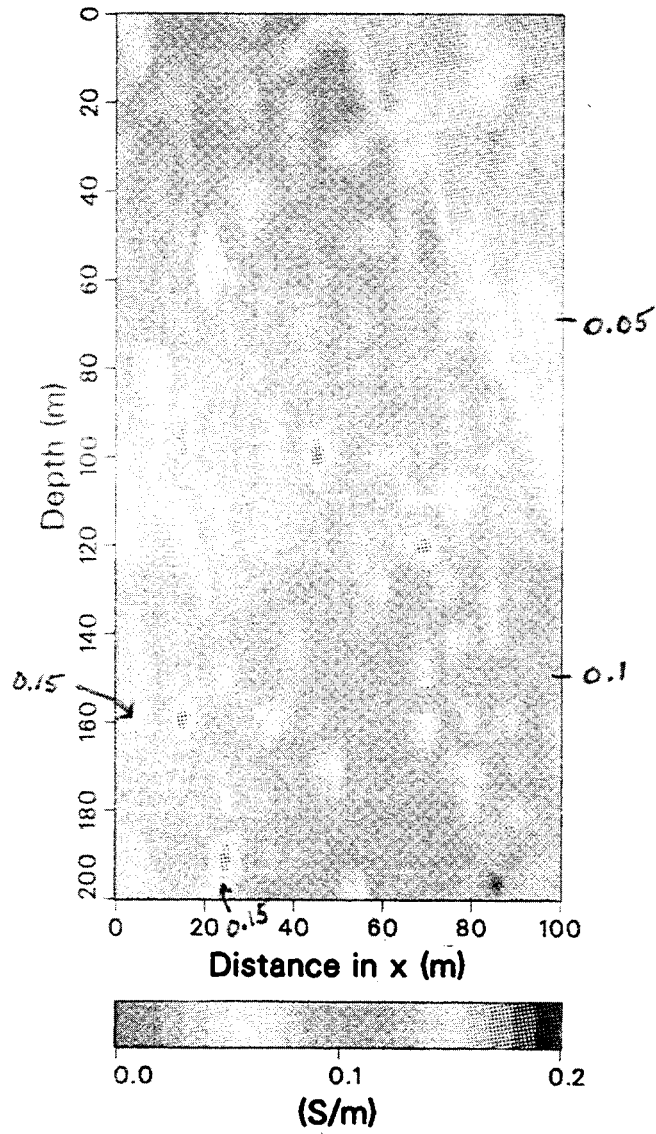


Figure 7. Conductivity tomogram after 40 iterations.

Wave-Field Ray Paths

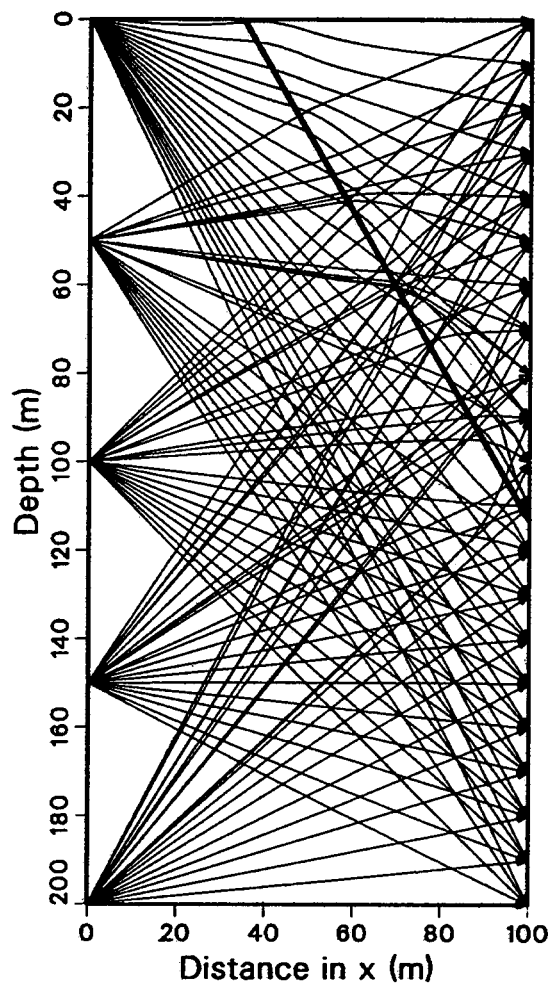


Figure 8. Raypaths from five sources at $z=0$, 50, 100, 150, and 200 m to 21 receivers, after 68 iterations.

Conductivity Tomogram

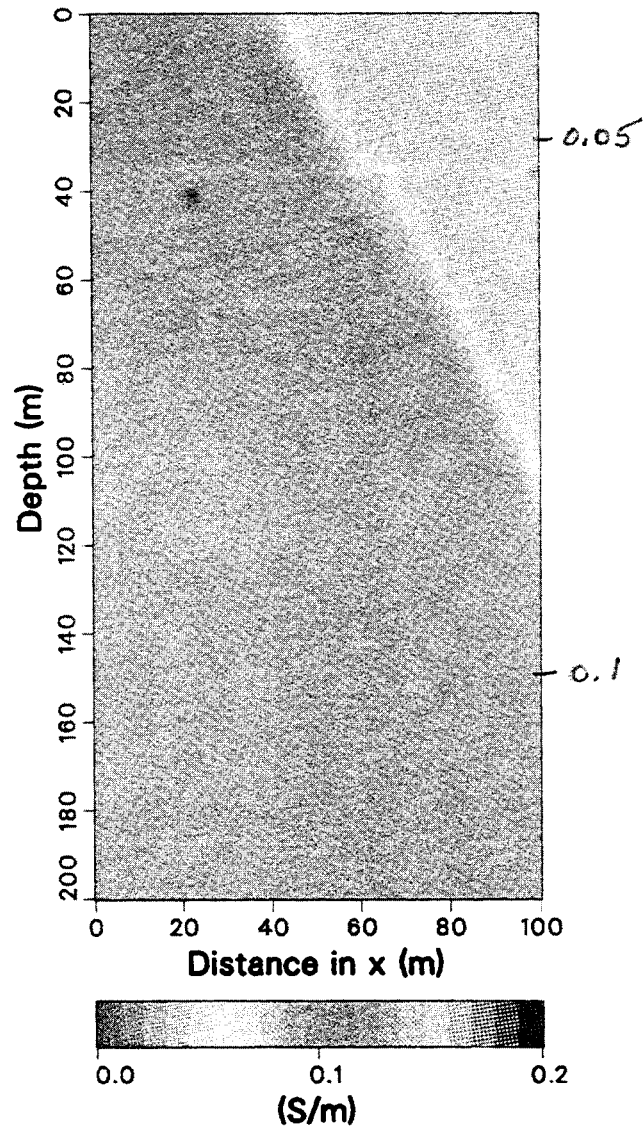


Figure 9. Conductivity tomogram after 68 iterations.

Richmond Field Station Wellfield

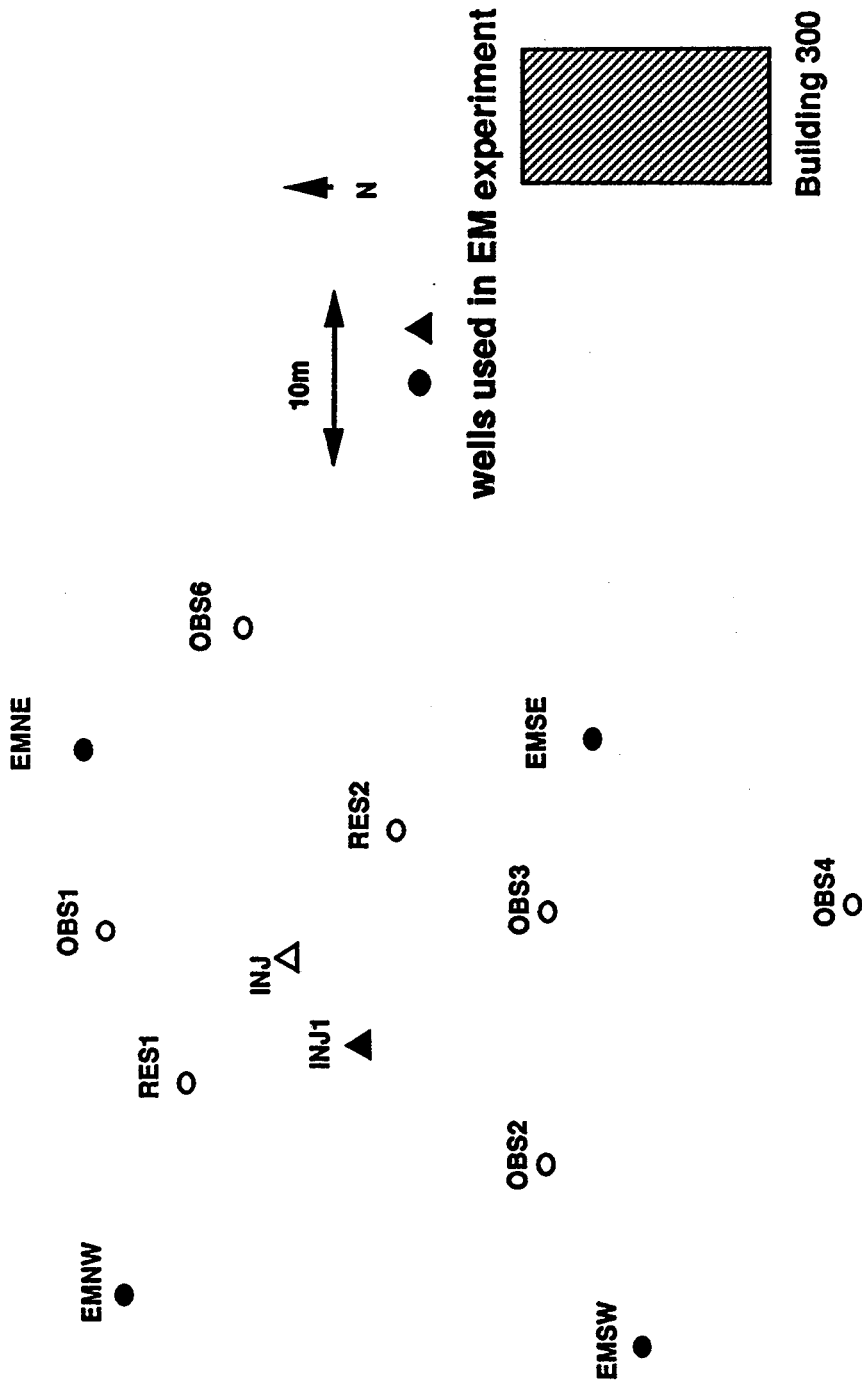


Figure 10. Location map building 300 well field at the Richmond Field Station

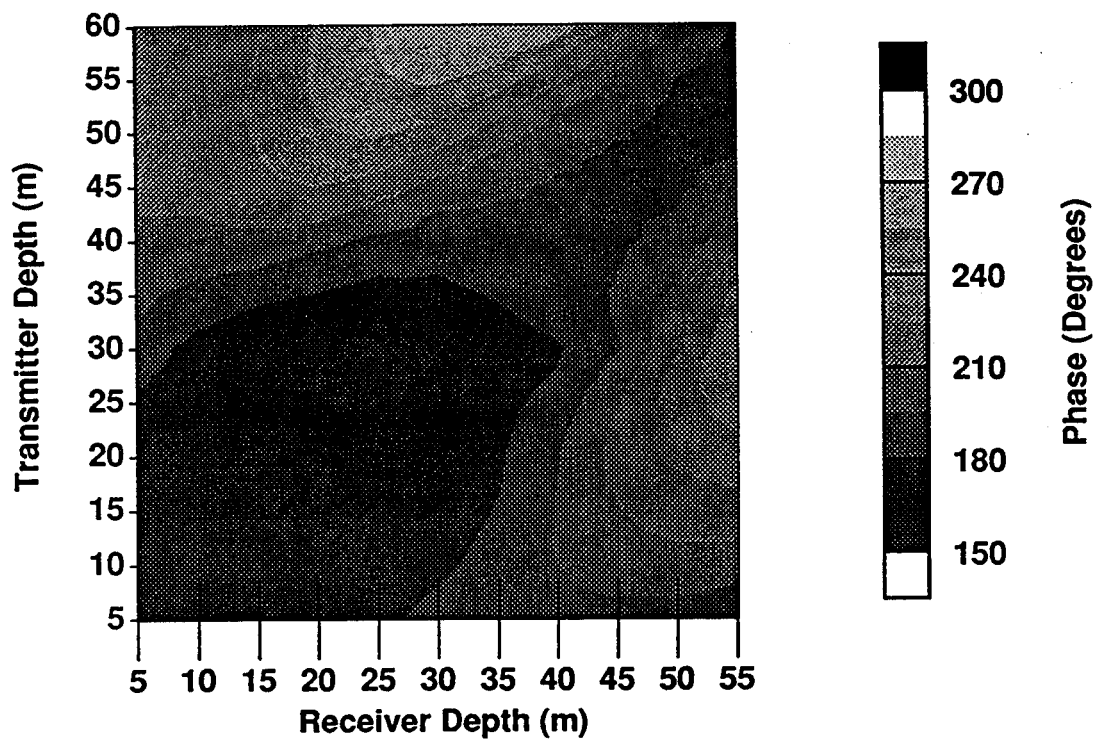
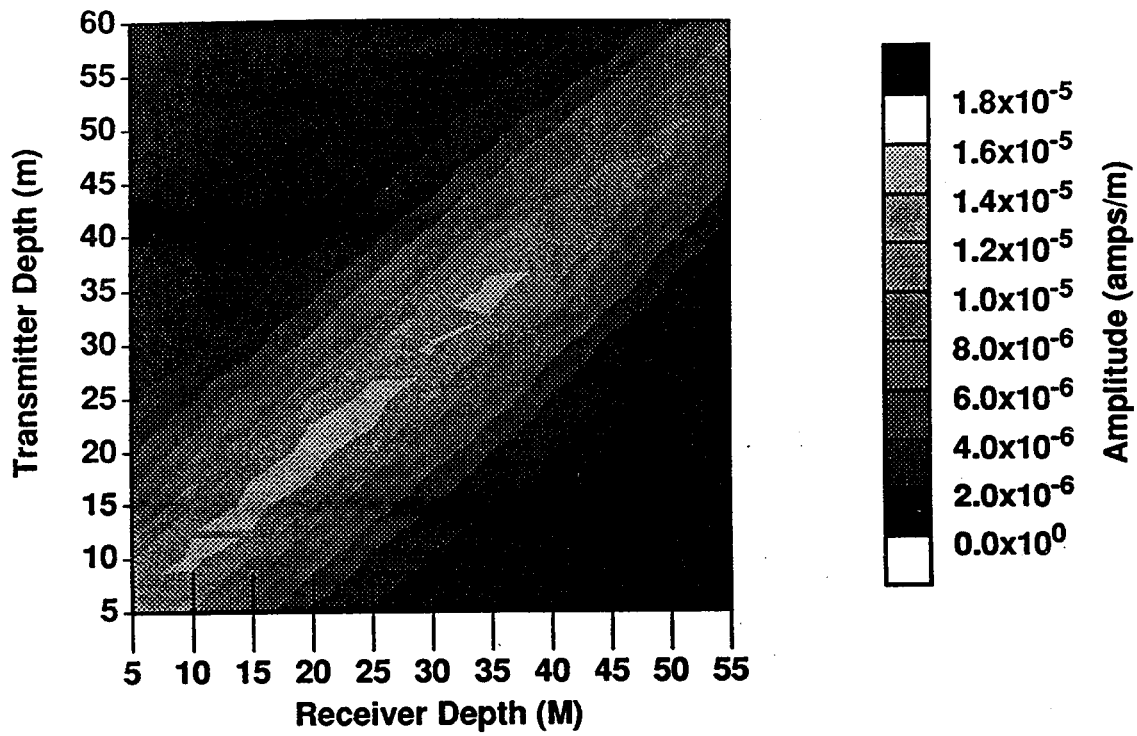


Figure 11. EMNW data amplitude and phase prior to injection. Each line on the receiver axis represents an individual profile of data in transmitter depth.

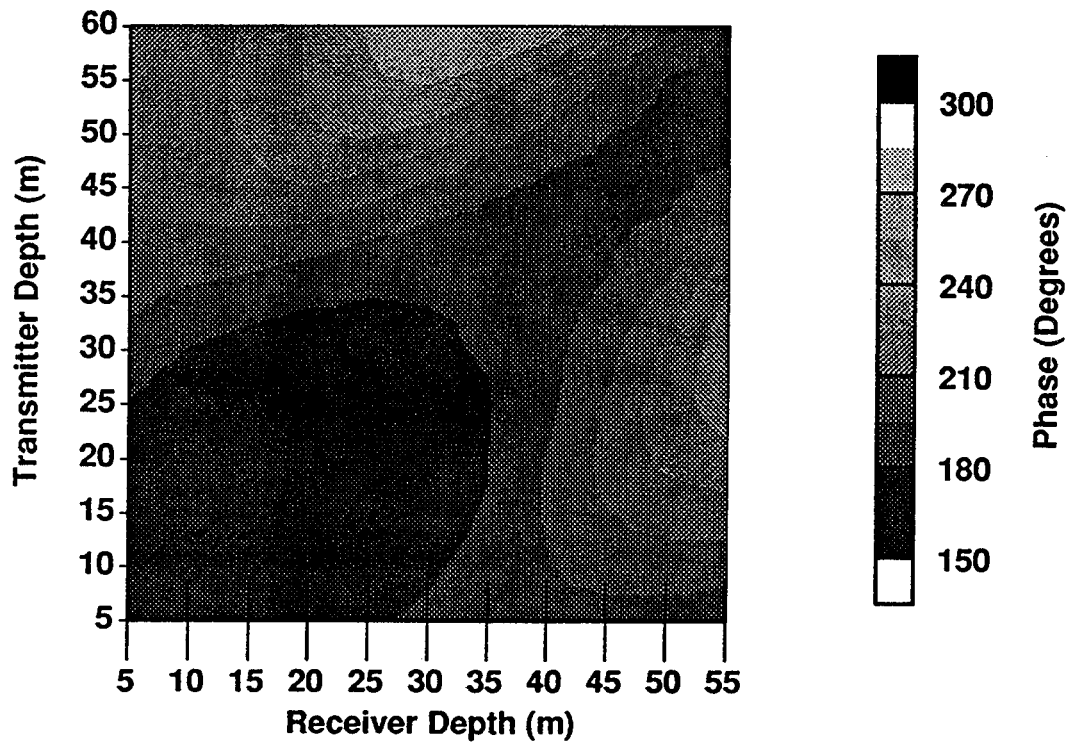
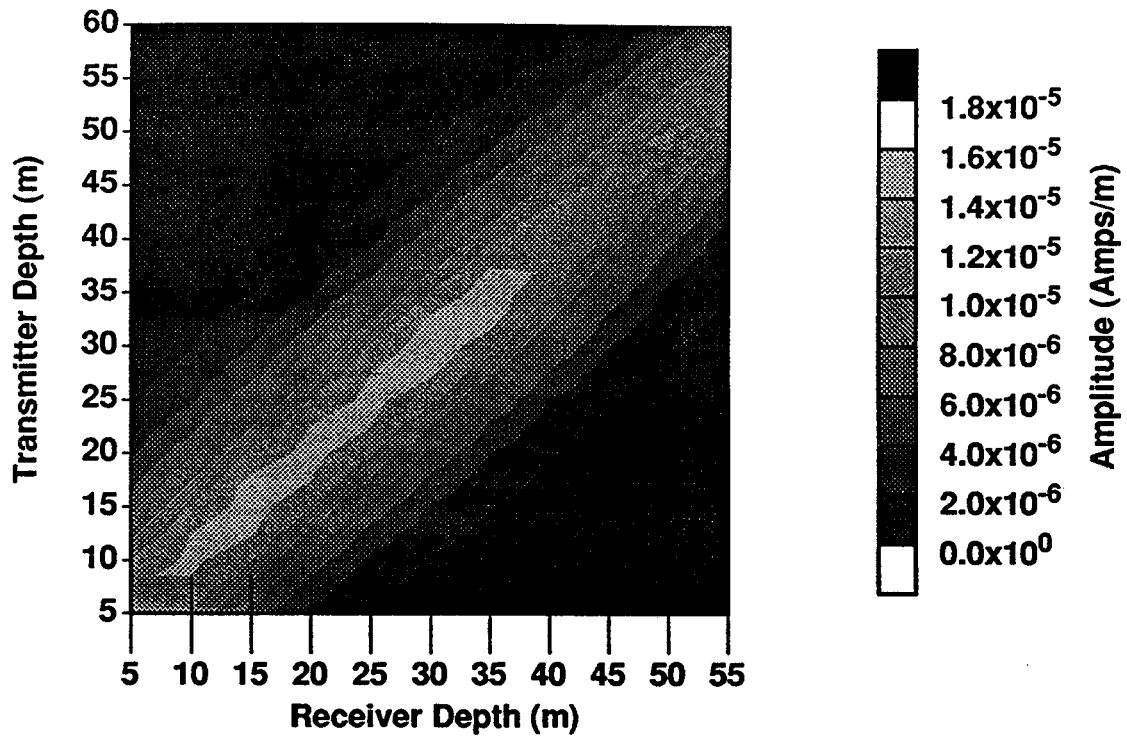


Figure 12. EMNW data amplitude and phase after injection. Each line on the receiver axis represents an individual profile of data in transmitter depth.

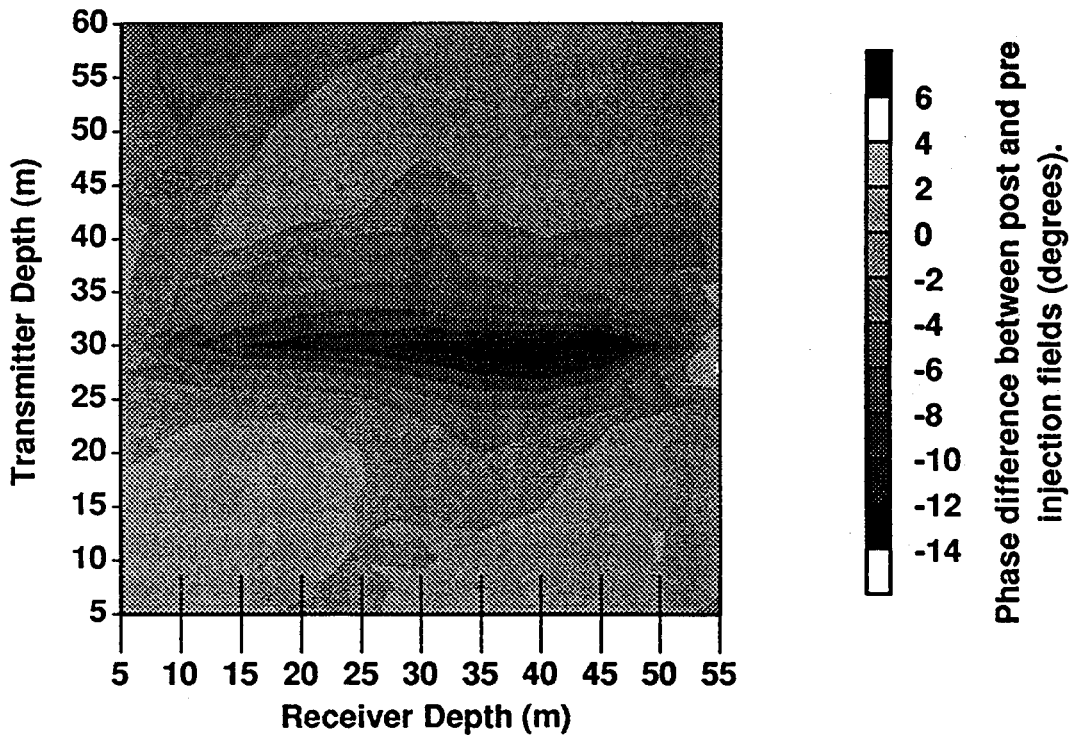
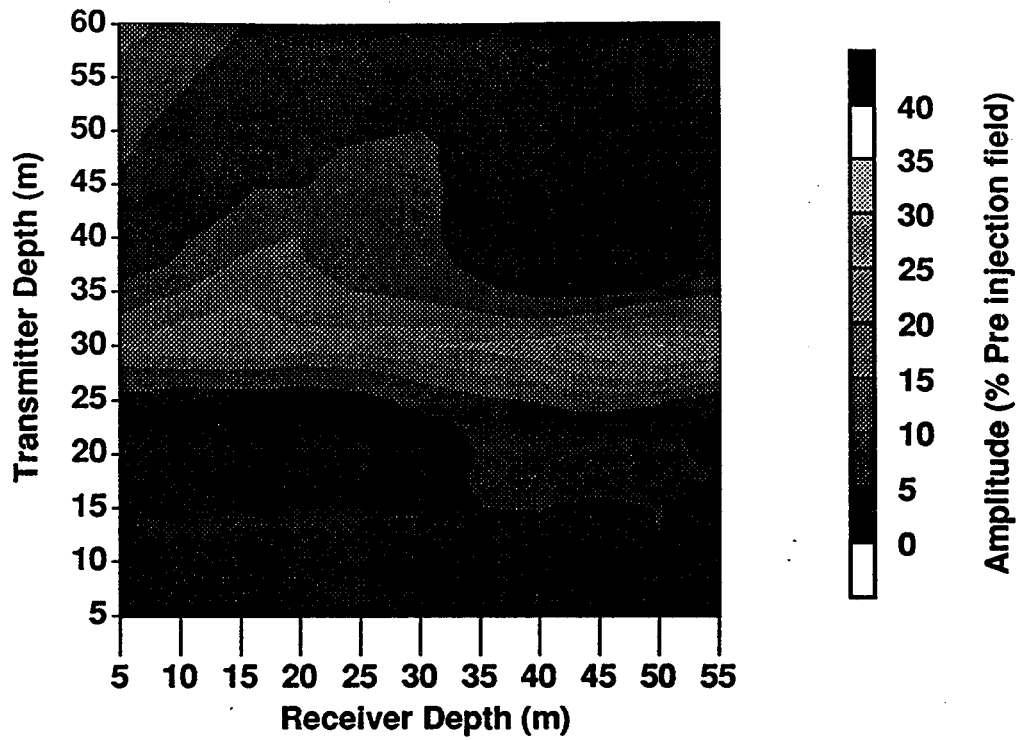


Figure 13. Secondary fields in borehole EMNW. Each line on the receiver axis represents an individual profile of data in transmitter depth.

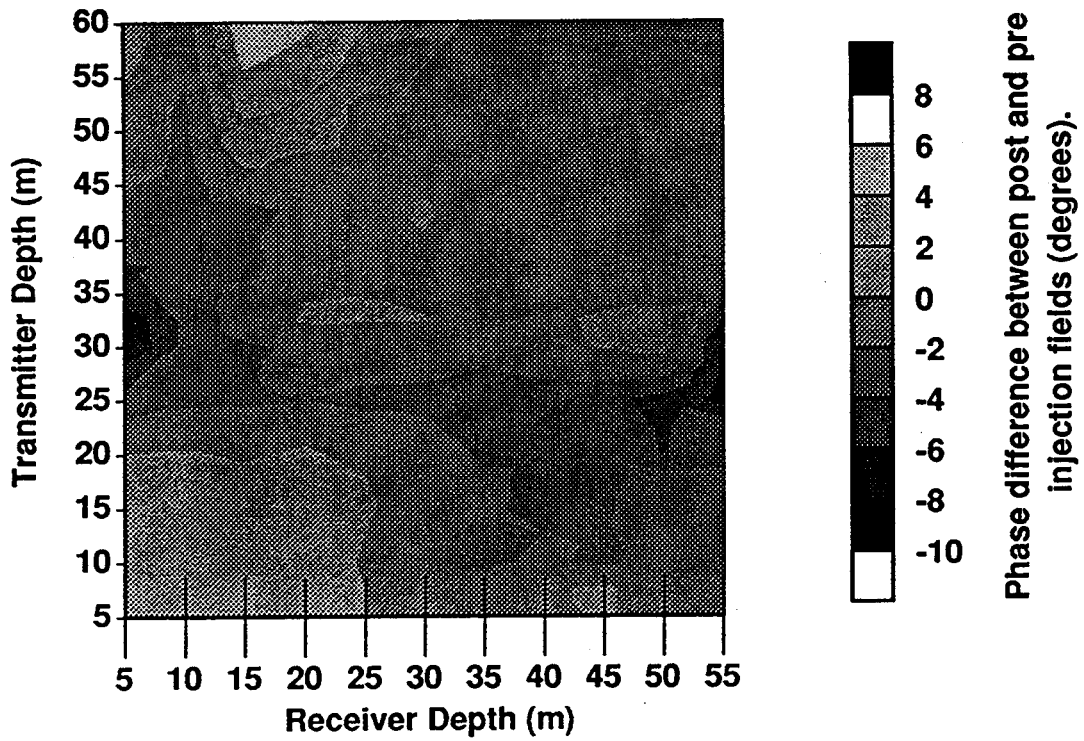
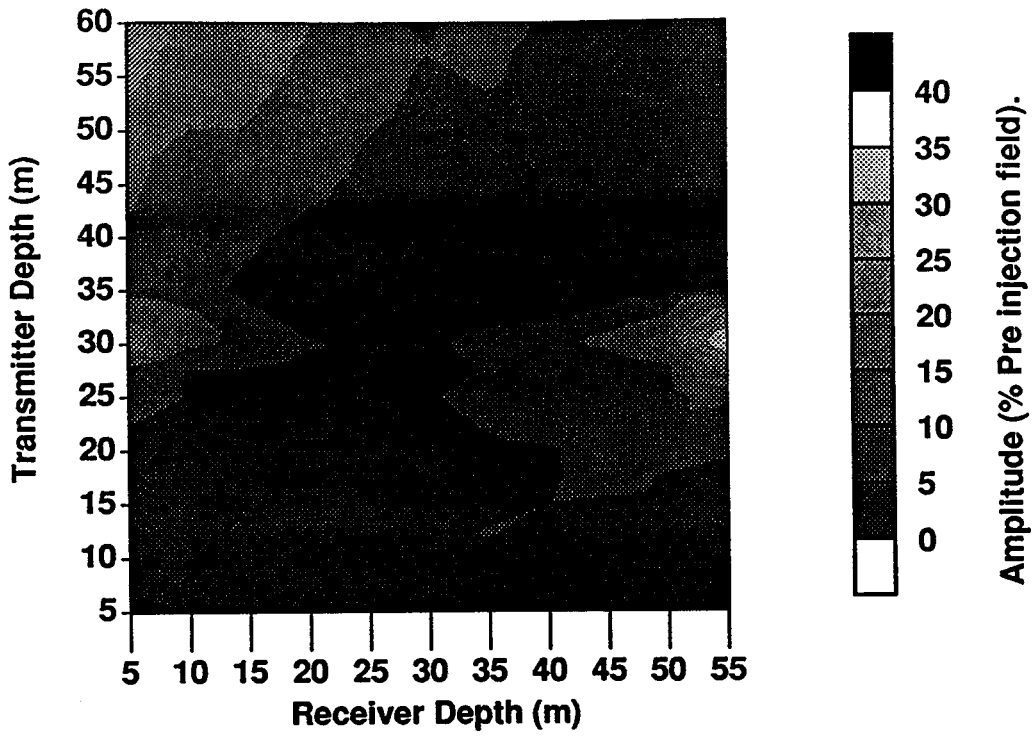


Figure 14. Secondary fields in borehole EMSW. Each line on the receiver axis represents an individual profile of data in transmitter depth.

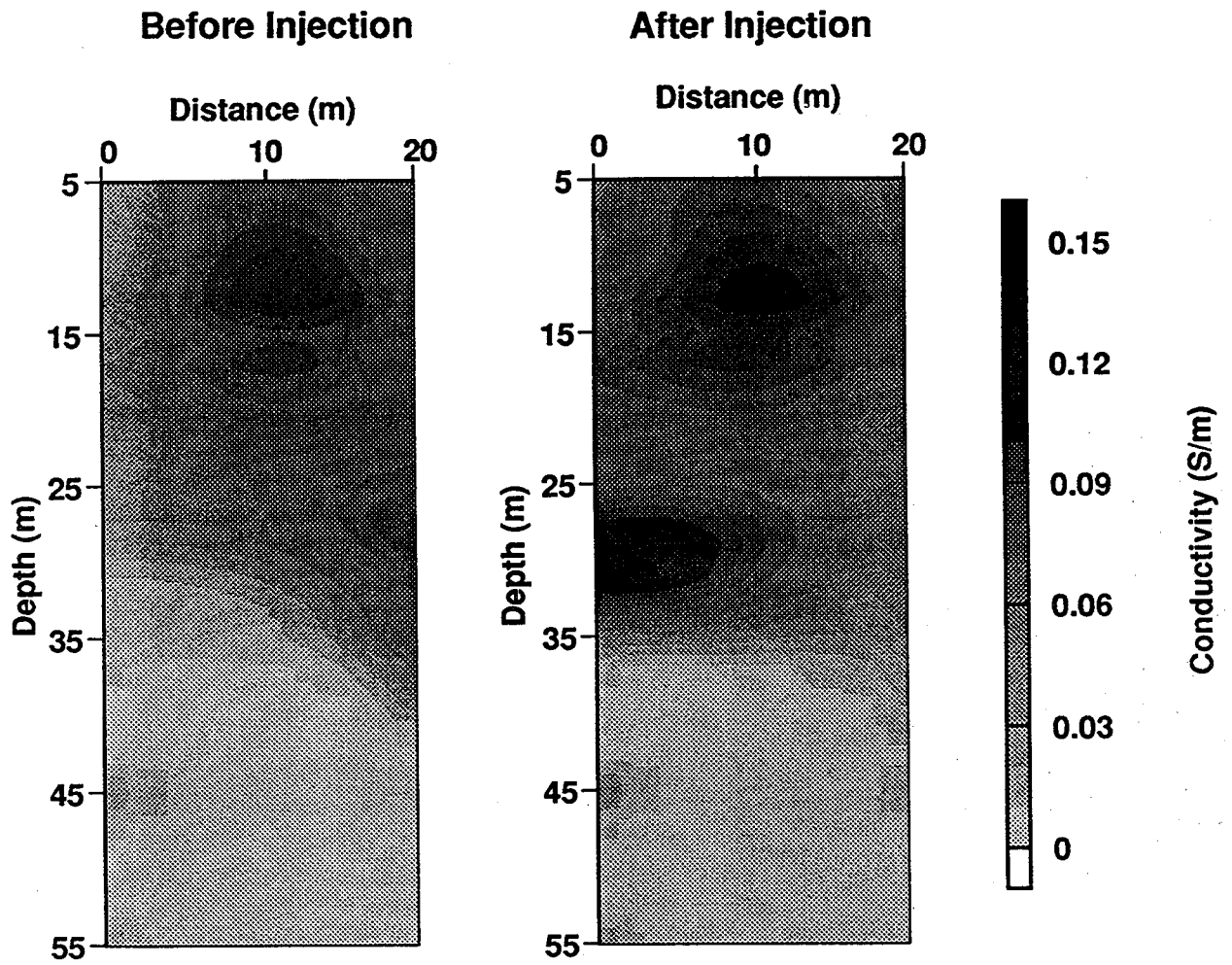


Figure 15. Iterative Born inversion of EMNW data.

Difference in Conductivity (Post - Pre Injection)

ENNW

Distance (m)

0 10 20

5 15 25 35 45 55

Depth (m)

EMNE

Distance (m)

0 13 26

5 15 25 35 45 55

EMSW

Distance (m)

0 13 26

5 15 25 35 45 55

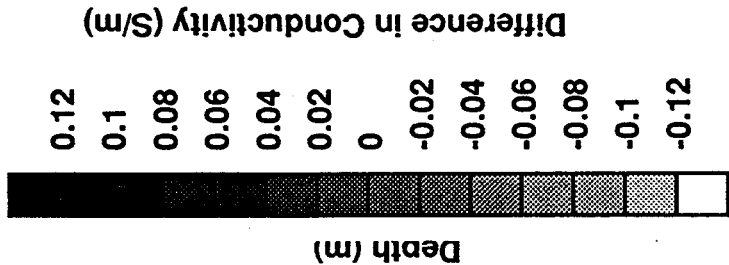


Figure 16. Difference in conductivity between the post-injection and pre-injection images for the ENNW, EMNE and EMSW data sets.

